Title

Mapping Molecular Structure of Protein Locating on Nanoparticles with Limited Proteolysis

Journal

Analytical Chemistry, 91(6)

ISSN

0003-2700

Authors

Duan, Yaokai
Liu, Yang
Coreas, Roxana
et al.

Publication Date

2019-03-19

DOI

10.1021/acs.analchem.9b00482

Peer reviewed

HHS Public Access

Author manuscript

Anal Chem. Author manuscript; available in PMC 2020 March 19.

Published in final edited form as:

Anal Chem. 2019 March 19; 91(6): 4204–4212. doi:10.1021/acs.analchem.9b00482.

Mapping Molecular Structure of Protein Locating on Nanoparticles with Limited Proteolysis

Yaokai Duan[†], **Yang Liu**[‡], **Roxana Coreas**[‡], and **Wenwan Zhong**[*,†,‡]

[†]Department of Chemistry, University of California, Riverside, California 92507, United States

[‡]Environmental Toxicology Graduate Program, University of California, Riverside, California 92507, United States

Abstract

The molecular structure of a protein could be altered when attached to nanoparticles (NPs), affecting the performance of NPs present in biological systems. Limited proteolysis coupled with LC-MS/MS could reveal the changes in protein structure when it binds to a variety of entities, including macro-molecules and small drugs, but has not yet been applied to study protein-NP interaction. Herein, adsorption of proteins, transferrin and catalase, on the polystyrene (PS) or iron oxide (IO) NPs was analyzed with this method. Both increased and decreased proteolytic efficiency in certain regions on the proteins were observed. Identification of the peptides affected by protein-NP interaction led to proper prediction of alterations to protein function as well as to colloidal stability of NPs. Overall, the present work has demonstrated the utility of limited proteolysis in helping elucidate the potential biological outcomes of the protein-NP conjugate, obtaining knowledge to guide improvement of the rational design of the protein conjugated NPs for biomedical applications, and to understand the biological behaviors of the engineered NPs.

Protein adsorption on the surface of engineered nanoparticles (NPs) unintentionally exposed to biological systems is inevitable.[1–5] On the other hand, intentionally attaching specific proteins (i.e. antibodies) on NPs as the target recognition moieties has also been used to achieve active targeting and assist delivery of NPs for therapeutic purposes.[6–8] While the adsorbed protein corona could be beneficial to the outcomes of the NPs by keeping the NPs from being cleared by the innate immune system;[9–11] structural changes, e.g. unfolding, fibrillation and aggregation,[12–14] could occur to the protein after binding to the NPs, and induce negative impacts on the protein-NP conjugates.[7,15,16] For example, protein unfolding can expose the originally buried cryptic epitopes to induce immune clearance of the NPs and

[*]**Corresponding Author**: Wenwan.zhong@ucr.edu.

Author Contributions

All authors have given approval to the final version of the manuscript.

ASSOCIATED CONTENT

Supporting Information

The proteolysis efficiency of protein-NP; normalized band intensity of transferrin/apo-transferrin; the proteolysis process monitored by fluorescamine labeling; intrinsic fluorescence and CD spectra of protein with NP; the size of peptides generated by limited proteolysis; the peak area of peptides identified; Cat activity test; the melting curves of transferrin/apo-transferrin with IONPs, the supernatant of IONPs, or different amount of Fe^{3+} ions; the melting curves of HSA with IONPs; the RA value plot of transferrin with or without IONPs; hydrodynamic diameter and normalized particle concentration of PSNPs or IONPs with protein or peptide. The Supporting Information is available free of charge on the ACS Publications website.

hinder cellular uptake;[17–19] and the functional motif of a protein may be blocked by the NPs, causing impedance to its capability of target recognition or enzymatic activity.[20] Thus, to improve our understanding of the biosafety of the engineered NPs, and to guide rational design of the protein-NP conjugates used for biomedical applications, it is necessary to learn the details about the orientation and conformation of the protein present on NP surface.[21]

The methods currently used to study protein conformation change include circular dichroism (CD), intrinsic fluorescence spectroscopy, thermo stability test, fluorogenic dye labeling, and Fourier-Transform InfraRed (FTIR) spectroscopy.[22–27] Although these are universal methods applicable for most proteins, they could not provide structural information at the amino acid residue level. On the other hand, immuno-probes specifically targeting one protein motif have been applied to map the orientation of the protein on the surface of NPs.[6,28–30] However, this method cannot assess changes to other parts of the protein other than the targeted motif, and the availability of the immune-probe also restricts its application on diverse proteins. In some cases, more detailed information (i.e. residues level) of a protein can be studied via distance-sensitive probing methods, e.g. fluorescence resonance energy transfer (FRET) or radical reactions,[31,32] while it is quite challenging to introduce the probes at the desired residues. Nuclear magnetic resonance (NMR) or mass spectrometry (MS) coupled with bio-orthogonal labeling, cross-linking, or hydrogen/deuterium exchange (HDX), can also provide detailed molecular structural information, e.g. which residues are more solvent accessible and whether two residues are in proximity.[33–36] Nevertheless, the reactivity of these labeling reagents are quite limited, requiring excess reagents and long reaction times; and the reversible reaction as well as the covalent labels on amino acid residues enhance difficulty in MS analysis.

Limited proteolysis coupled with LC-MS/MS have been successfully applied to study protein-protein (PPIs), protein-drug, and protein-metabolite interactions.[37–40] Taking advantage of the protease that has high reactivity and selectivity towards specific residues, limited proteolysis employs a very short digestion step to cleave the peptides that are on the surface of a proteins and accessible to the solvent, without large scale disruption of protein conformation. Identifying the resultant peptides in MS can then reveal changes in protein's solvent accessible surface area (SASA) caused by interacting entities, which could reflect alteration to protein conformation and orientation in the binding complex.

The capability of limited proteolysis to provide a genuine snapshot of protein structure makes it an ideal approach to explore protein structure when located on the surface of NPs. Moreover, the short reaction time minimizes protein unfolding caused by extensive digestion. This can prevent displacement of the adsorbed proteins by the digested peptides from the carrier surface,[41,42] which are the major concerns involved in the pioneer works that applied completed proteolysis on proteins (α-synuclein and carbonic anhydrase II) adsorbed on gold or silica NPs using long digestion times (i.e. 2 hr, 4 hr).[43,44] Herein, the present work tested limited proteolysis on several protein-NP pairs, the interaction of which was revealed in our previous studies.[45,46] By comparing the solvent accessible peptides obtained during the 5–10 minutes short protease digestion with or without NPs, we identified the detailed protein structure changes induced by adsorption to the NPs; and the attained information helped interpret alterations in protein activity and NP colloidal stability.

Experimental Section

Chemicals and Biochemicals.

Fluorescamine, Triton X-100, iodoacetamide (IAM) and all proteins including trypsin were obtained from Sigma-Aldrich (St. Louis, MO, USA). Hydrogen peroxide (H_2O_2), dimethyl sulfoxide (DMSO), Coomassie brilliant blue R-250, formic acid, acetonitrile (ACN), urea, dithiothreitol (DTT), anhydrous sodium phosphate dibasic, sodium chloride, ammonium bicarbonate, acrylamide, sodium dodecyl sulfate (SDS) and ammonium persulfate were purchased from Fisher Scientific (Waltham, MA, USA). The Laemmli sample buffer (2×) was obtained from Bio-Rad (Hercules, CA, USA). All proteins were purchased from Sigma-Aldrich (St. Louis, MO). Ultrapure water with electric resistance larger than 18.2 MΩ was produced by the Milli-Q water purification system (Millipore, Billerica, MA, USA).

Nanoparticles (NPs).

The carboxylated polystyrene nanoparticles (PSNPs) with a hydrodynamic diameter (HD) of 48 ± 7 nm and ζ potential of −87 ± 11 mV, and the silica nanoparticles (SiNPs) with a HD of 66 ± 10 nm and ζ potential of −50 ± 4 mV, were purchased from Polysciences (Warrington, PA, USA) and nanoComposix (San Diego, CA, USA), respectively. Iron oxide NPs (IONPs) were obtained from the HSPH-NIEHS Nanosafety Center of the NHIR consortium, and suspended in 1×PBS (pH 7.4) based on the suggested method.[47] The ζ potential and HD of IONPs were 63 ± 18 mV and 237 ± 99 nm, respectively.

Trypsin limited proteolysis and in-gel visualization.

Proteins (0.2 mg/ml) were incubated with 0.43 mg/ml of the PSNPs, or 0.66 mg/ml SiNPs, or 0.10 mg/ml of the IONPs in 1×PBS buffer (10 mM phosphate buffer at pH 7.4, with 137 mM NaCl and 2.7 mM KCl) for 1 hr at 37 °C. Then, trypsin was added in a 1:50 mass ratio. After 10 minutes incubation at 37 °C, the 2× Laemmli sample buffer was added in a 1:1 ratio to terminate the digestion. Proteins in 1×PBS without the presence of NPs were also processed in the same manner and used as controls. To visualize the digestion efficiency, 20 μL of each mixture was loaded and separated in SDS-PAGE (4% polyacrylamide stacking gel, 12% polyacrylamide separation gel, with 0.1% SDS). Coomassie brilliant blue R-250 was used to stain the gel, and the band intensities were quantified using ImageJ.[39] The band intensity of each protein incubated with NPs was normalized to that of the corresponding control, to represent the relative digestion efficiency changed by NPs.

Catalase activity assay.

In a 16 × 125 mm borosilicate glass tube containing 100 μl of 0.5 mg/ml catalase in 1×PBS buffer, 100 μl of 1% Triton X-100 and 200 μl of 30% H_2O_2 were added. After mixing, the height of the foam layer generated by oxygen was recorded every 20s.[40] The plot of the foam layer height vs. reaction time ($V_{initial}$) was used to obtain the slope of the initial linear range of this kinetic curve, which was used to represent the activity of catalase (EC_0, in mm/s). To measure the activity influenced by the PSNPs, 0.5 mg/ml of catalase was incubated with either 0.215 or 0.43 mg/ml of the PSNPs for 1 hr at 37 °C, followed by the

addition of Triton X-100 and H_2O_2. Then, foam heights were recorded, and the catalase activity (EC_{PSNP}) calculated from $V_{initial}$ was normalized by dividing EC_0.

Limited proteolysis.

Trypsin and chymotrypsin were used to perform limited digestion, separately. The same procedure in the previous part was used, except for chymotrypsin in which 1 mM calcium was added. Following a digestion period of 10 or 60 minutes, 8 M urea was added in a 1:1 ratio to terminate reaction, followed with DTT to a final concentration of 5 mM. The mixture was incubated at 56 °C for 30 minutes. After the mixture was cooled to room temperature, 10 mM of IAM was added and incubated for 20 minutes in the dark. The whole solution was filtered through a 30 kDa Amicon centrifugal filter in 14,000 ×g for 10 minutes, and the particles remaining on top of the filter were washed with 1×PBS (pH 7.4) twice to remove the peptides. All of the filtrates containing cleaved peptides were collected and diluted with 50 mM ammonium bicarbonate. More trypsin or chymotrypsin was added in a mass ratio of 1:50 (protease : protein). After overnight digestion at 37 °C, all those solutions were lyophilized and desalted.

LC-MS/MS.

Peptides generated in both filtrate and supernatant were analyzed in a CapLC system (Waters Corporation, Milford, MA, USA) connected to a Finnigan LTQ mass spectrometer (Fisher Scientific, Maltham, MA, USA) with an ESI nanospray source. The desalted and lyophilized samples were dissolved in 0.1% formic acid (FA) aqueous solution, and then loaded into a homemade reverse phase (RP) separation column (75 μm i.d. × 10 cm). The column was packed with 5 μm C18 silica beads (Dr. Maisch HPLC GmbH, Germany). Gradient elution was generated using 0.1% FA in water as Solvent A and 0.1% FA in ACN as Solvent B. The separation was started at a flow rate of ~ 200 nL/min (after flow splitting) with 2% B for 20 minutes, followed by a linear gradient increase to 50% B during a period of 60 minutes. After that, 80% B for 20 minutes and 2% B for 30 minutes were used to wash and equilibrate the columns. Positive mode full MS scan was carried out within a mass range of 300–2000 m/z and MS/MS was operated in a data-dependent mode. Collision induced dissociation (CID) with 35% collision energy was used to activate fragmentation.

Data Searching and Analysis.

MSGF Plus was used to identify peptide sequences using the sequences of catalase (bovine), serum albumin (human), and transferrin (human) downloaded from UniProt. These sequences with reverse order were used as decoys. Iodoacetamide of cysteine was defined as constant modification, and oxidation of methionine was defined as dynamic modifications. The cutoff for parent ion tolerance was set to be 3 Da, and the Q value that represent false discovery rate (FDR) was set to be smaller than 0.01. The spectra count (SC) of each peptide was used to quantify the cutting sites that generate this peptide. The relative abundance (RA) of the cutting site i was calculated by Equation 1:

$$\%RA = \frac{SC_i}{\sum SC} \times 100\% \quad (1)$$

Aggregation assessment by size and concentration measurement of NPs.

PSNPs (0.43 mg/ml), or IONPs (0.1 mg/ml), were incubated with 0.2 mg/ml proteins in 10 mM 1×PBS buffer (pH 7.4) at 37 °C for 1 hr. After proper dilution with 1×PBS (100–2000 fold), nanoparticle tracking analysis (NTA) was used to measure the HD and particle counts of the NPs. For each sample, the particle count was normalized by dividing the count of the NPs control. On the other hand, the same concentration of protein was initially digested with trypsin (1:50 mass ratio) overnight at 37 °C, and then incubated with 0.43 mg/ml of the PSNPs or 0.1 mg/ml IONPs in 1×PBS (pH 7.4) for 1 hr at 37 °C. Afterwards, the HD and particle counts of the NPs in these mixtures were measured by NTA.

Thermal stability screening.

The same incubation step as stated above was conducted by mixing 0.43 mg/ml PSNPs or 0.1 mg/ml of IONPs and 0.2 mg/ml of the protein at 37 °C for 1 hr. Next, SYPRO Orange dye was added to the solution at a final concentration of 4×. Then, the mixture was transferred into the CFX Real-Time PCR instrument (Bio-Rad) and subject to a temperature gradient that increased from 37 to 98 °C with an incubation period of 20 s at each temperature before recording the fluorescence intensity excited by a laser at 488 nm and collected through an emission filter of 515–545 nm.

Results and Discussion

Limited proteolysis for study of protein on NPs.

We previously reported a high throughput screening method relying on fluorescamine to label the solvent accessible free amines on proteins to explore changes in protein conformation during NP binding.[45,46] Both hindrance and enhancement of fluorescamine labeling have been observed, suggesting that the surface lysine residues could be blocked; or more of the originally buried lysine residues could be exposed, upon interaction with the NPs. Although the fluorescence-based measurement allows for rapid assessment of protein-NP binding events in a high-throughput manner, this method could not reveal the peptides for which the labeling situation has been altered by the interaction.

Fluorescamine labeling targets the solvent accessible lysines on protein surface. Similarly, during limited proteolysis, which takes place in few minutes instead of several hours, the protease only has enough time to cut the solvent accessible amino acids locating on protein surface. We expect binding to NPs could change the number of protease accessible cutting sites (PACS): some of the original cutting sites may become inaccessible if buried in the binding interface; contrarily, new sites may be exposed if protein unfolding occurs due to NPs binding. Then, it is possible that we could use limited proteolysis to identify the regions on the protein that are affected by binding to the NPs.

As illustrated in Figure 1, limited proteolysis starts with incubating the protein with the NPs of interest for a certain period of time. We chose 1 hr in the present work, which has been proved to be long enough to reach binding equilibrium,[48,49] so that the experimental results will be consistent and not affected by the dynamic binding process. Then the sample is subject to limited proteolysis. The resultant peptides with Mw < 30 kDa can be removed

from the bulky, undigested part of the protein using an Amicon centrifugal filter with a molecular weight cutoff (MWCO) of 30 kDa, and identified by LC-MS/MS. The number of each cleaved peptide can be semi-quantitatively represented by the relative abundance (RA) value. Plotting this RA value against the position of the amino acid residue (AA#) on the protein, we can identify amino acid regions that exhibit changes in the RA values after protein binding to the NPs, and provide information to map the molecular structure, mainly orientation and unfolding, of the protein adsorbed on the nanoparticles. For example, an increase in the RA value upon protein-NPs interaction could indicate alterations in protein conformation; while a decrease could reflect the orientation of the protein when located on the surfaces of NPs. Either case can potentially affect the functionality or stability of proteins in solutions.

Binding to NPs changes protein digestion efficiency.

In our previous work, we screened the binding between various proteins and SiNPs or PSNPs using the fluorescamine assay. These two NPs were chosen in the study owing to their wide applications in biomedical research and negligible interferences to fluorescence.[45,46] We found that: transferrin and catalase exhibited much enhanced labeling when interacting with the PSNPs, but no change with the SiNPs. In addition, the labeling profile for human serum albumin (HSA) did not show much difference with either type of NPs. The difference could be attributed to the physicochemical properties of the NPs and proteins. However, fluorescamine labeling cannot reveal information about the regions on the proteins being affected by NP binding, preventing further interpretation of the labeling results. Since the lysine residue targeted by fluorescamine is the cutting site of trypsin, we investigated whether the trypsin digestion efficiency of these proteins would also be changed by the NPs. Then, analyzing the peptides produced from limited proteolysis could possibly reveal information about the binding interface and disclose changes to protein conformation.

We first focused on transferrin. Transferrin functionalized PSNPs have been developed as drug delivery platforms for active targeting of cancer cells, utilizing the affinity binding of transferrin for its receptor (TfR) that is overly expressed on the surfaces of certain types of cancer cells.[50] It has been found that, the TfR targeting ability is highly dependent on the proper orientation and conformation of transferrin on the surface of NPs.[51,52] The structure stability and conformation of transferrin with or with no Fe^{3+} bound are quite different, with TfR only able to recognize the Fe-bound form. Thus, we included both transferrin (60% bound to iron) and apo-transferrin (no iron bound) in this work to see whether they show different outcomes upon NP binding with the well-characterized variations in their structural property.

Interestingly, we found that, incubation with the PSNPs substantially increased the digestion efficiency for transferrin, leading to ~ 55% and 65% more loss of the intact transferrin with 10- and 60-min trypsin treatment, respectively, compared to the protein alone when analyzing the protein samples by SDS-PAGE (Figure 2A&B; Figure S-1&2). More substantial changes (~70% and 80%) were observed with apo-transferrin, which is considered as less rigid in structure than transferrin due to the lack of iron binding. Using fluorescamine to label the N-terminus generated from proteolytic cleavage, we evaluated the

digestion rate by monitoring the time-dependent increase in fluorescence, which should be proportional to the number of the produced N-termini. In accordance with the PAGE results, incubation with the PSNPs led to 4 and 6.5 folds increase in the digestion rate of transferrin and apo-transferrin, compared to the protein only sample (Figure S-3).

In contrast, for the protein-NP pairs that did not show any changes in their fluorescamine labeling profiles, i.e. transferrin with the SiNPs and HSA with either NPs, the same proteolytic treatment did not induce noticeable changes in digestion efficiency (Figure S-1). These phenomena also proved that the protease activity was not affected by the NPs. Comparable digestion phenomena were also observed with another protease, chymotrypsin: enhanced digestion of transferrin but no change for HSA when incubated with the PSNPs (Figure S-4).

The larger degree of protease digestion occurred to transferrin or apo-transferrin when bound to the PSNPs could be the result of reduction in protein structure stability. We thus evaluated protein unfolding using SYPRO Orange staining, the fluorescence of which can be turned on when inserted into the hydrophobic region of a protein structure. We employed a real-time PCR instrument to monitor the fluorescence of SYPRO Orange when increasing the temperature of the protein sample to induce protein unfolding, which exposed more hydrophobic regions for the dye to bind. The temperature at which the protein starts to unfold, termed the melting temperature, T_m, was measured as that resulting in a peak value in derivative of fluorescence. Indeed, the T_m of transferrin/apo-transferrin shifted from 60 °C to 45–50 °C when incubated with the PSNPs, indicating decreased stability (Figure 2C). The measurement of intrinsic fluorescence also showed dramatic decreases in the intrinsic fluorescence of transferrin/apo-transferrin, suggesting that the binding to PSNPs could quench the intrinsic fluorescence of protein (Figure S-5). Meanwhile, the decrease of CD signal at 220 nm was also observed in the presence of the PSNPs, confirming the occurrence of protein conformation change (Figure S-6).

Taken together, these results support that, binding to the PSNPs could change the protease digestion efficiency for transferrin or apo-transferrin, and such a change may be due to protein conformation change as revealed by well adopted techniques. The enhanced digestion efficiency makes it feasible to obtain detectible amounts of peptides with the short-term proteolytic digestion, i.e. limited proteolysis. Identifying the affected peptides may reveal exactly what parts of the protein are affected by NPs binding.

Mapping the molecular structure of transferrin on PSNP by limited proteolysis.

Analysis of the protein fragments attained during a 10-min trypsin digestion by SDS-PAGE showed that, majority of the cleaved fragments were smaller than 20 kDa (Figure S-7). Therefore, we used an Amicon ultra-centrifugal filter with a molecular-weight-cut-off value (MWCO) of 30 kDa to separate the cleaved peptides from the undigested parts of the protein. The protein fragments collected in filtrate were subjected to a regular trypsin digestion process to produce smaller peptides identifiable in our LC-MS/MS set-up. Then, any changes in the quantities and/or identities of the PACS induced by binding to the PSNP would reveal the surface blocked or exposed upon binding. The semi-quantitative MS method of spectral counting was used to obtain the relative abundance (RA) of each peptide

among all identified by LC-MS/MS. The average of RAs among three repeats were plotted according to their location (represented by amino acid #) on the protein, and compared between samples.

As for the result, we noticed that, large differences in the RA values were observed for various peptide regions in both transferrin and apo-transferrin before and after binding to the PSNPs (Figure 3A), which were also verified by comparing the peak areas of selected peptide regions in MS^1 (Figure 3B). The regions of AA #100–120 and #400–450 for both transferrin and apo-transferrin, as well as # 550–580 for apo-transferrin (shaded in blue in Figure 3A) showed significant increases in their RA values, supporting that these regions could be exposed more upon interaction with the PSNPs and become more protease accessible. These regions contain multiple β-sheets and α-helix moieties (Figure S-8), and their unfolding agreed with the CD spectra changes presented above.

Interestingly, although the overall proteolytic efficiency of transferrin/apo-transferrin was increased upon binding to the PSNPs, we observed dramatic decreases in the RA values for the NPs surface. Mapping these peptide regions on the crystal structure of transferrin, we found that these sequences are involved in the binding interface between transferrin and TfR (Figure 3C). If the binding site for TfR is not exposed outward when transferrin is anchored on the NP surface, TfR targeting could be inhibited. It has been previously reported that the low ratio (≈10%) of transferrin with the proper orientation locating on the PSNP surface reduced the TfR targeting capability of the transferrin-PSNP conjugate compared to the protein alone.[30]

Activity alteration caused by molecular structural change in catalase when adsorbed on PSNPs.

Catalase is another protein that showed enhanced susceptibility to proteolytic digestion after binding to the PSNPs (Figure S-1): ~30% more of catalase was digested by trypsin within 10 min following incubation with the PSNPs and analysis by SDS-PAGE with Coomassie blue staining. Similar to the case of transferrin on the PSNPs, limited proteolysis by both trypsin and chymotrypsin showed consistent increase in the RA values for the N-terminus (shaded in red) and AA# 240–260 (shaded in green); and the RA values for the AA # 350–380 range (in blue) exhibited some decrease (Figure 4A&B). The changes of RA values were again verified by quantifying the MS^1 peak areas of the identified peptides (Figure 4C). The N-terminus of catalase (Figure 4D, in red) is mostly buried inside the neighboring subunit when four identical subunits form the native tetramer. The increased RA values in this region upon binding to the PSNPs suggests that the regions of AA# 140–160 and # 480–500 (shaded in red in Figure 3A). The reduced protease accessibility hints the possibility of them being blocked by the PSNPs during protein-NP interaction. Four tryptophan residues locate in or near these regions. Their proximity to the PSNP surface may induce the observed decrease in protein intrinsic fluorescence shown in Figure S-5.

These results indicate that, transferrin or apo-transferrin experienced substantial conformation change upon binding to the PSNPs. In some part of the protein, more cleavage sites were exposed to the protease. Blockage of protein surface by the NPs was observed as well, which could be related to how the protein is oriented on the tetramer structure could be

disrupted. On the other hand, the region of AA # 350–380 may locate at the protein-NP binding interface and thus its RA values dropped. This region locates close to the heme group that is linked to Y357 (Figure 4E).

Since both the tetramer structure and the heme group are critical to the function of catalase in catalyzing metabolite or toxin oxidation by hydrogen peroxide, PSNP binding that disrupted the tetramer structure and occurred close to the heme group may be detrimental to catalase's enzymatic function. Therefore, we used the foam test to measure the activity of catalase.[53] In this test, catalase catalyzes the decomposition of H_2O_2 in a solution containing Triton X-100; and the produced O_2 would form a visible foam layer in the test-tube. The height of the foam layer is proportional to the amount of O_2, and thus increased linearly with the reaction time (Figure S-9). The slope of this kinetic curve can be used to evaluate enzymatic activity. As we expected, incubation with 0.215 and 0.43 mg/ml PSNPs decreased the activity of catalase by 20% and 50%, respectively (Figure 4F). Interestingly, this adverse effect on enzyme activity could be alleviated by adding another protein (e.g. ovalbumin, transferrin, and lysozyme) to the protein - PSNPs mixture (Figure 4G), further confirming that the activity loss was due to adsorption of catalase on PSNPs surface. The added protein may displace catalase off the PSNPs surface, thus resuming its activity.

Immobilizing catalase on NPs has been employed to facilitate application of catalase in industrials.[54,55] Our results point out that a strategic selection of the NPs is desired for such applications because immobilization of catalase on the surface of NPs may reduce its enzymatic activity, which can be better guided with the molecular structure information revealed by this limited proteolysis method.

Limited proteolysis at elevated temperature.

The above results prove that limited proteolysis can be applied to analyze proteins showing substantial increase in their proteolytic efficiency when binding to the NPs, and reveal the protein regions being affected by NP binding, helping interpret potential impacts on protein function. Owing to the inherent magnetism and good biocompatibility, IONPs is one of the most studied and promising inorganic nanocarriers for biomedical applications.[57,58] Thus, it would be interesting to learn more details regarding the structural change and orientation of protein adsorbed on the IONPs by limited proteolysis.

However, during our initial screening, we observed that the proteolytic efficiency for transferrin or apo-transferrin was decreased upon binding to the IONPs. As shown in Figure 5A (also Figure S10), transferrin/apo-transferrin were relative resistant to a short time proteolysis at 37 °C, and there was barely any observable band intensity difference for transferrin/apo-transferrin incubated with or without the IONPs. Meanwhile, CD measurements confirmed that binding with IONPs did not induce dramatic unfolding of transferrin/apo-transferrin, despite a small decrease (10%) in the signal at 220 nm produced by the α-helix structures of the proteins (Figure S-11), consistent with previous report.[56] In these cases, substantial blockage of protein surface by the IONPs may make fewer amino acid residues accessible to the protease. Unlike increased proteolysis efficiency of transferrin induced by PSNPs, the decreased proteolysis efficiency induced by IONPs posts a challenge

to limited proteolysis, because the few peptides produced could prevent clear identification of the sequences of which the protease accessibility are affected by IONPs binding.

To enlarge the difference and obtain more peptides by limited proteolysis, we stimulated protein unfolding by heating the protein solution to 60 °C. The activity of trypsin can be enhanced as well at this elevated temperature. As shown in Figure 5B, at this temperature the protein band intensity showed some decrease after 10- or 60- min trypsin treatment. But when they were incubated with the IONPs, less protein was digested, as observed from the higher protein band intensities compared to the no-NP control. Due to the lack of Fe^{3+} ions to stabilize the structure, apo-transferrin was digested faster than transferrin, thus more significant differences in its digestion efficiency with or without the NPs were visualized on the SDS-PAGE result: the intact apo-transferrin remained after 10- or 60- min digestion with the IONPs in present was 1.6 and 5.3 folds of that of the protein alone (Figure 5C). Fluorescamine labeling of the N-terminus produced by proteolysis also confirmed that IONP binding inhibited proteolytic digestion of transferrin and apo-transferrin by 15% and 30%, respectively (Figure 5D). The decreased digestion efficiency of transferrin/apo-transferrin with IONPs was not caused by the activity loss of trypsin, as no change was observed in digestion of HSA with or without the IONPs (Figure 5B).

Decreased proteolysis efficiency induced by IONPs binding indicated that the proteins may be stabilized by the NPs. Indeed, as shown in Figure 6A, the T_m of apo-transferrin increased from 58 and 67 °C to 82 °C after incubated with the IONPs. A similar effect was also observed for transferrin (Figure S-12). The stabilization was not a result of binding to the free Fe^{3+} cations potentially dissolved from the NPs: when using only the supernatant of the IONPs to incubate with the proteins, no change in the T_m was observed (Figure 6B, Figure S-12B). In addition, increasing the concentration of the IONPs while keeping the concentration of transferrin/apo-transferrin constant increased the intensity of the T_m peak at 82 °C and decreased the original peaks at 58 and 67 °C. The T_m peak at lower temperatures completely disappeared with 100 μg/ml IONPs, probably as an outcome of all protein molecules being bound to the NPs at this IONPs concentration (Figure 6A, Figure S-12C). Moreover, similar thermal stability enhancement effect can be achieved by incubating transferrin/apo-transferrin with Fe^{3+} ions (Figure S-14). This suggests that the iron binding motif on transferrin/apo-transferrin could direct the specific binding to the IONPs, further stabilizing the structures of transferrin and apo-transferrin. On the other hand, for HSA that showed unchanged proteolysis efficiency when incubated with IONPs (Figure 5B), its thermal stability was not affected by the IONPs either (Figure S-13).

With more peptides cleavable under the heating condition, we carried out limited proteolysis at 60 °C to digest the free or IONP-bound transferrin or apo-transferrin, and collected the peptides for LC-MS/MS analysis. Agreeing with the results shown in Figure 5 and 6, no obvious increased digestion was noticed, owing to the enhanced thermal stability (Figure 7A, Figure S-15). Binding to the IONPs substantially decreased the RA values of transferrin/apo-transferrin at multiple regions across the whole sequence of the protein, though the decrease was more discernable for apo-transferrin. The MS^1 peak area of the identified peptides also confirmed such decreases, with the most significant decrease found in the regions of AA#47–60, 237–251, 554–564, and the C-terminus (Figure 7B), indicating that

these regions might be blocked by the IONPs. After mapping the identified peptides on the crystal structure of transferrin with TfR (Figure 7C), we see that these regions were not involved in the binding interface of transferrin and TfR, unlike in the situation of binding to the PSNPs.

Aggregation of NPs induced by protein unfolding.

Protein adsorption on NPs may change protein conformation and thus its function. Meanwhile, the colloidal stability and biocompatibility of the NPs may also be changed if protein binding quenches the surface charge of the NPs, or the unfolding of proteins expose hydrophobic regions to facilitate aggregation, etc.[13,14,59] With the molecular structure of proteins on the surface of NPs revealed by limited proteolysis, these potential outcomes could be predicted and/or better understood.

Limited proteolysis revealed that apo-transferrin would unfold after adsorbed on the PSNPs. Indeed, severe particle aggregation was observed for the PSNPs when incubated with apo-transferrin (Figure 8), as shown by the dramatic decrease in the total particle counts and the enlarged particle HD. On the contrary, apo-transferrin adsorption on the IONPs induced no aggregation (Figure 8). Similar phenomena were also observed for other NP-protein mixtures: since the tetramer structure of catalase was disrupted by the PSNPs, severe aggregation of the PSNPs mediated by the adsorbed catalase was observed; but HSA, the structure of which was not affected by the IONPs, did not induce obvious IONPs aggregation (Figure S-16).

Both apo-transferrin unfolding and the catalase tetramer structure being disrupted by the PSNPs can expose hydrophobic regions (i.e. red region in Figure 4). Thus, we attribute the correlation between protein unfolding and NPs aggregation to the bridging effect between the binding motif and the exposed hydrophobic region. This hypothesis is supported by the result of incubating the peptides generated by digesting either catalase or apo-transferrin with the PSNPs, which did not induce the aggregation of PSNPs (Figure S-16). After digestion, the linkages between the binding motif and the hydrophobic region of the protein were cleaved, eliminating the bridging effect that induced aggregation of NPs.

Conclusions

The above results and discussions have demonstrated that limited proteolysis is suitable for characterizing the molecular structure, like the orientation and unfolding, of the protein adsorbed on NPs. These insights can help illustrate the potential outcomes to the protein as well as to the protein-NP complex. Among the protein-NP systems we tested, both protein unfolding and stabilization were observed and rationalized through limited proteolysis, with the former increasing the proteolysis efficiency and the number of peptides identified, and the latter showing the completely opposite effects. Location of the affected peptides on protein also reveal the potential impedance to protein function. Furthermore, substantial protein unfolding indicates the possibility of protein-mediated NPs aggregation.

Still, the precision of this method is limited by the distribution of cutting sites of the protease; and definitive interpretation of protein structural changes induced by NPs can be

challenging. But we anticipate that, since it is fast and simple, limited proteolysis can be a quick survey tool to gain better understanding of the impact of the adsorbed protein layer, i.e. protein corona, to the behaviors of NPs entering biological systems. The information can also guide the design of protein-NP conjugates with increased stability and good retention of protein functionality for biomedical research and applications.

Supplementary Material

Refer to Web version on PubMed Central for supplementary material.

ACKNOWLEDGMENT

Research reported in this publication was supported by the National Institute of Environmental Health Sciences of the National Institutes of Health under Award Number U01ES027293 as part of the Nanotechnology Health Implications Research (NHIR) Consortium. IONPs used in the research presented in this publication have been procured/developed, characterized, and provided by the Engineered Nanomaterials Resource and Coordination Core established at Harvard T. H. Chan School of Public Health (NIH grant # U24ES026946) as part of the Nanotechnology Health Implications Research Consortium. R. Coreas was thankful to the support from the Research Training Grant in Environmental Toxicology from the National Institute of Environmental Health Sciences (T32ES018827). The content is solely the responsibility of the authors and does not necessarily represent the official views of the National Institutes of Health.

REFERENCES

(1). Björnmalm M; Thurecht KJ; Michael M; Scott AM; Caruso F ACS nano 2017, 11, 9594–9613. [PubMed: 28926225]

(2). Jiang W; Von Roemeling CA; Chen Y; Qie Y; Liu X; Chen J; Kim BY Nat. Biomed. Eng 2017, 1, 0029.

(3). von Roemeling C; Jiang W; Chan CK; Weissman IL; Kim BY Trends. Biotechnol 2017, 35, 159–171. [PubMed: 27492049]

(4). Shi J; Kantoff PW; Wooster R; Farokhzad OC Nat. Rev. Cancer 2017, 17, 20. [PubMed: 27834398]

(5). Szebeni J; Muggia F; Gabizon A; Barenholz Y Adv. Drug Delivery Rev 2011, 63, 1020–1030.

(6). Tonigold M; Simon J; Estupiñán D; Kokkinopoulou M; Reinholz J; Kintzel U; Kaltbeitzel A; Renz P; Domogalla MP; Steinbrink K; Lieberwirth I; Crespy D; Landfester K; Mailänder V Nat. Nanotechnol 2018, 13, 862–869. [PubMed: 29915272]

(7). Mitragotri S; Burke PA; Langer R Nature reviews. Drug discovery 2014, 13, 655–672. [PubMed: 25103255]

(8). Ray M; Lee Y-W; Scaletti F; Yu R; Rotello VM Nanomedicine (London, U. K.) 2017, 12, 941–952.

(9). Oh JY; Kim HS; Palanikumar L; Go EM; Jana B; Park SA; Kim HY; Kim K; Seo JK; Kwak SK; Kim C; Kang S; Ryu J-H Nat. Commun 2018, 9, 4548. [PubMed: 30382085]

(10). Tenzer S; Docter D; Kuharev J; Musyanovych A; Fetz V; Hecht R; Schlenk F; Fischer D; Kiouptsi K; Reinhardt C Nat. Nanotechnol 2013, 8, 772. [PubMed: 24056901]

(11). Van Hong Nguyen B-JL Int. J. Nanomed 2017, 12, 3137.

(12). Naganathan AN; Doshi U; Fung A; Sadqi M; Muñoz V Biochemistry 2006, 45, 8466–8475. [PubMed: 16834320]

(13). Shang W; Nuffer JH; Dordick JS; Siegel RW Nano Lett 2007, 7, 1991–1995. [PubMed: 17559285]

(14). Deng ZJ; Liang M; Monteiro M; Toth I; Minchin RF Nat. Nanotechnol 2011, 6, 39. [PubMed: 21170037]

(15). Agrahari V; Agrahari V; Mitra AK Ther. Delivery 2016, 7, 257–278.

(16). Wilhelm S; Tavares AJ; Dai Q; Ohta S; Audet J; Dvorak HF; Chan WC Nat. Rev. Mater 2016, 1, 16014.

(17). Mortimer GM; Butcher NJ; Musumeci AW; Deng ZJ; Martin DJ; Minchin RF ACS nano 2014, 8, 3357–3366. [PubMed: 24617595]

(18). Lynch I; Dawson KA; Linse S Sci. Signaling 2006, 2006, pe14-pe14.

(19). Corbo C; Molinaro R; Tabatabaei M; Farokhzad OC; Mahmoudi M Biomater. Sci 2017, 5, 378–387. [PubMed: 28133653]

(20). Walczyk D; Bombelli FB; Monopoli MP; Lynch I; Dawson KA J. Am. Chem. Soc 2010, 132, 5761–5768. [PubMed: 20356039]

(21). Kamerzell TJ; Esfandiary R; Joshi SB; Middaugh CR; Volkin DB Adv. Drug Delivery Rev 2011, 63, 1118–1159.

(22). Kim Y; Ko SM; Nam J-M Chem. - Asian J 2016, 11, 1869–1877. [PubMed: 27062521]

(23). Azad VJ; Kasravi S; Zaienabad HA; Aval MMB; Saboury AA; Rahimi A; Falahati M J. Biomol. Struct. Dyn 2016, 35, 1. [PubMed: 26727155]

(24). Raoufi M; Hajipour MJ; Kamali Shahri SM; Schoen I; Linn U; Mahmoudi M Nanoscale 2018, 10, 1228. [PubMed: 29292453]

(25). Vitali M; Rigamonti V; Natalello A; Colzani B; Avvakumova S; Brocca S; Santambrogio C; Narkiewicz J; Legname G; Colombo M Biochim. Biophys. Acta 2018, 1862, 1556–1564.

(26). Zaman M; Ahmad E; Qadeer A; Rabbani G; Khan RH Int. J. Nanomed 2014, 9, 899.

(27). Fang X; Zheng Y; Duan Y; Liu Y; Zhong W Anal. Chem 2019, 91, 482–504. [PubMed: 30481456]

(28). Herda LM; Hristov DR; Lo Giudice MC; Polo E; Dawson KA J. Am. Chem. Soc 2016, 139, 111–114. [PubMed: 28005336]

(29). Lara S; Alnasser F; Polo E; Garry D; Lo Giudice MC; Hristov DR; Rocks L; Salvati A; Yan Y; Dawson KA ACS nano 2017, 11, 1884–1893. [PubMed: 28112950]

(30). Kelly PM; Åberg C; Polo E; O'connell A; Cookman J; Fallon J; Krpetić Ž; Dawson KA Nat. Nanotechnol 2015, 10, 472. [PubMed: 25822932]

(31). Tureček F; Julian RR Chem. Rev 2013, 113, 6691–6733. [PubMed: 23651325]

(32). Faulón Marruecos D; Schwartz DK; Kaar JL Curr. Opin. Colloid Interface Sci 2018, 38, 45–55.

(33). Xu Y; Matthews S Top. Curr. Chem 2013, 335, 97–119. [PubMed: 21928013]

(34). Shrivastava S; Nuffer JH; Siegel RW; Dordick JS Nano Lett 2012, 12, 1583–1587. [PubMed: 22296027]

(35). Zeng S; Yu-ming MH; Chia-en AC; Zhong W Analyst 2014, 139, 1364–1371. [PubMed: 24482794]

(36). Srinivasu BY; Bose B; Mitra G; Kurpad AV; Mandal AK Langmuir 2017, 33, 8032–8042. [PubMed: 28727441]

(37). Piazza I; Kochanowski K; Cappelletti V; Fuhrer T; Noor E; Sauer U; Picotti P Cell 2018, 172, 358–372.e323. [PubMed: 29307493]

(38). Leuenberger P; Ganscha S; Kahraman A; Cappelletti V; Boersema PJ; von Mering C; Claassen M; Picotti P Science 2017, 355, eaai7825. [PubMed: 28232526]

(39). Feng Y; De Franceschi G; Kahraman A; Soste M; Melnik A; Boersema PJ; de Laureto PP; Nikolaev Y; Oliveira AP; Picotti P Nat. Biotechnol 2014, 32, 1036. [PubMed: 25218519]

(40). Lomenick B; Hao R; Jonai N; Chin RM; Aghajan M; Warburton S; Wang J; Wu RP; Gomez F; Loo JA Proc. Natl. Acad. Sci. U. S. A 2009, 106, 21984–21989. [PubMed: 19995983]

(41). Cedervall T; Lynch I; Lindman S; Berggård T; Thulin E; Nilsson H; Dawson KA; Linse S Proc. Natl. Acad. Sci. U. S. A 2007, 104, 2050–2055. [PubMed: 17267609]

(42). Chen F; Wang G; Griffin JI; Brenneman B; Banda NK; Holers VM; Backos DS Nat. Nanotechnol 2017, 12, 387–393. [PubMed: 27992410]

(43). Yang JA; Lin W; Woods WS; George JM; Murphy CJ J. Phys. Chem. B 2014, 118, 3559–3571. [PubMed: 24635210]

(44). Lundqvist M; Andresen C; Christensson S; Johansson S; Karlsson M; Broo K; Jonsson B-H Langmuir 2005, 21, 11903–11906. [PubMed: 16316131]

(45). Ashby J; Duan Y; Ligans E; Tamsi M; Zhong W Anal. Chem 2015, 87, 2213–2219. [PubMed: 25587850]

(46). Duan Y; Liu Y; Shen W; Zhong W Anal. Chem 2017, 89, 12160–12167. [PubMed: 29083159]

(47). DeLoid GM; Cohen JM; Pyrgiotakis G; Demokritou P Nat. Protoc 2017, 12, 355. [PubMed: 28102836]

(48). Vilanova O; Mittag JJ; Kelly PM; Milani S; Dawson KA; Rädler JO; Franzese G ACS Nano 2016, 10, 10842–10850. [PubMed: 28024351]

(49). Ashby J; Schachermeyer S; Pan S; Zhong W Anal. Chem 2013, 85, 7494–7501. [PubMed: 23859073]

(50). Pack DW; Hoffman AS; Pun S; Stayton PS Nat. Rev. Drug Discovery 2005, 4, 581. [PubMed: 16052241]

(51). Salvati A; Pitek AS; Monopoli MP; Prapainop K; Bombelli FB; Hristov DR; Kelly PM; Åberg C; Mahon E; Dawson KA Nat. Nanotechnol 2013, 8, 137. [PubMed: 23334168]

(52). Kelly PM; Aberg C; Polo E; O'Connell A; Cookman J; Fallon J; Krpetic Z; Dawson KA Nat. Nanotechnol 2015, 10, 472–479. [PubMed: 25822932]

(53). Iwase T; Tajima A; Sugimoto S; Okuda K; Hironaka I; Kamata Y; Takada K; Mizunoe Y Sci. Rep 2013, 3, 3081. [PubMed: 24170119]

(54). Singhal A; Morris VB; Labhasetwar V; Ghorpade A Cell Death Dis 2013, 4, e903. [PubMed: 24201802]

(55). Chan C; Sepunaru L; Sokolov SV; Katelhon E; Young NP; Compton RG Chem. Sci 2017, 8, 2303–2308. [PubMed: 28451333]

(56). Mahmoudi M; Shokrgozar MA; Sardari S; Moghadam MK; Vali H; Laurent S; Stroeve P Nanoscale 2011, 3, 1127–1138. [PubMed: 21210042]

(57). Bobo D; Robinson KJ; Islam J; Thurecht KJ; Corrie SR Pharm. Res 2016, 33, 2373–2387. [PubMed: 27299311]

(58). Ling D; Lee N; Hyeon T Acc. Chem. Res 2015, 48, 1276–1285. [PubMed: 25922976]

(59). Dominguez-Medina S; Kisley L; Tauzin LJ; Hoggard A; Shuang B; Indrasekara AS; Chen S; Wang LY; Derry PJ; Liopo A; Zubarev ER; Landes CF; Link S ACS Nano 2016, 10, 2103–2112. [PubMed: 26751094]

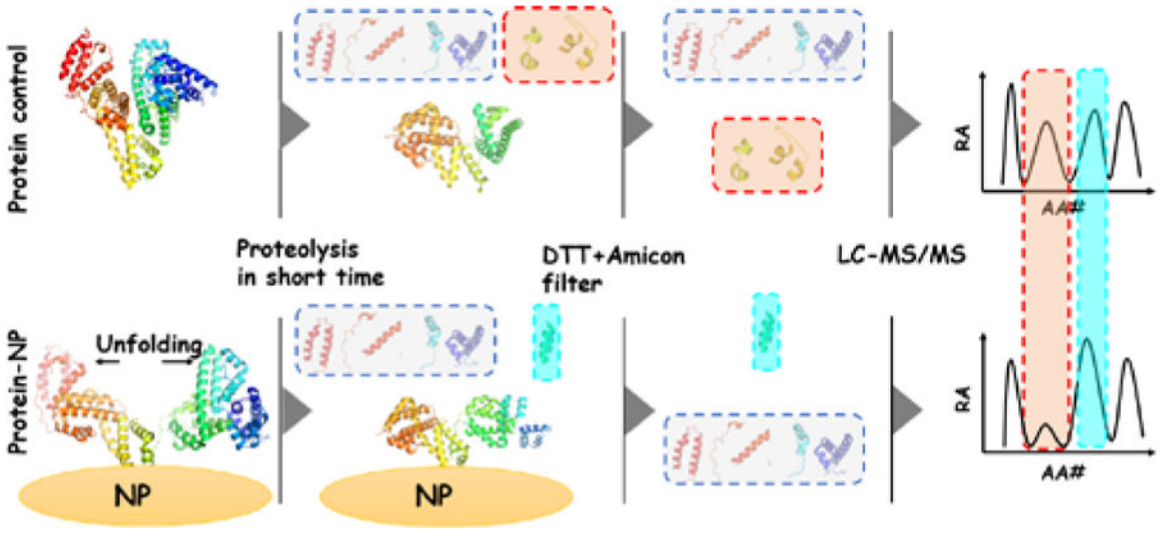

Figure 1.

Schematic illustration of the process of limited proteolysis for mapping the molecular structure of the protein displayed on NPs surface. Protein alone or incubated with the NP are subject to a very short duration of proteolysis in parallel; and the cleaved peptides are collected and identified by LC-MS/MS. NP interaction could induce protein unfolding to expose the inner part of protein, resulting in more peptides cleaved within the limited proteolysis period; and it could also block some peptides on the protein surface from being accessed by the protease, reducing their quantities found in MS analysis. The quantity of the peptide is represented semi-quantitatively by the value of RA. Plotting the RA values against the position of the amino acid residuse on the protein would reveal the regions being affected by protein-NP interaction.

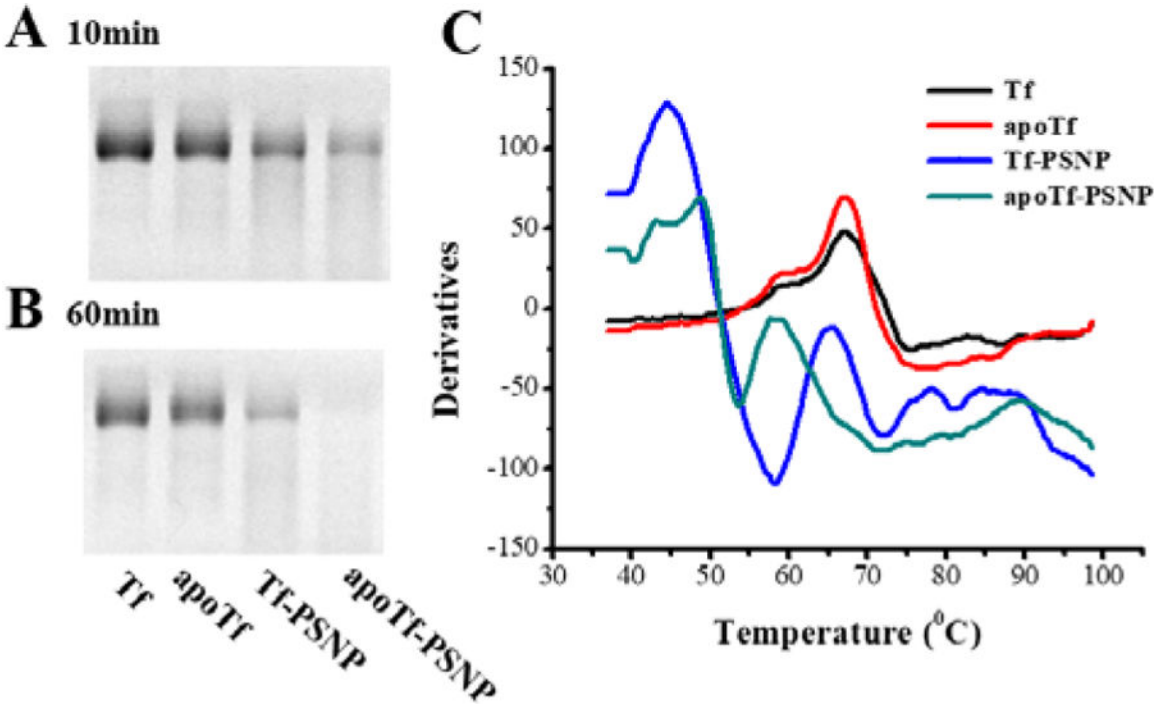

Figure 2.

The impact on the proteolysis efficiency and thermal stability of transferrin (Tf) and apo-transferrin (apoTf) upon adsorption onto the PSNPs. The amount of the protein remained after (A) 10- or (B) 60- min trypsin digestion was revealed by the intact protein band intensity obtained with SDS-PAGE. Trypsin was added in 1:50 mass ratio of the protein. (C) presents the melting curves of Tf/apoTf obtained through 4×SYPRO Orange staining, with the fluorescence collected using an excitation light at 488 nm and an emission filter of 515–545 nm. The Y-axis is the first order derivative of the fluorescence intensity. In all cases, Tf/apoTf with the concentration of 0.2 mg/ml were incubated with 0.43 mg/ml PSNPs at 37 °C for 1 hr.

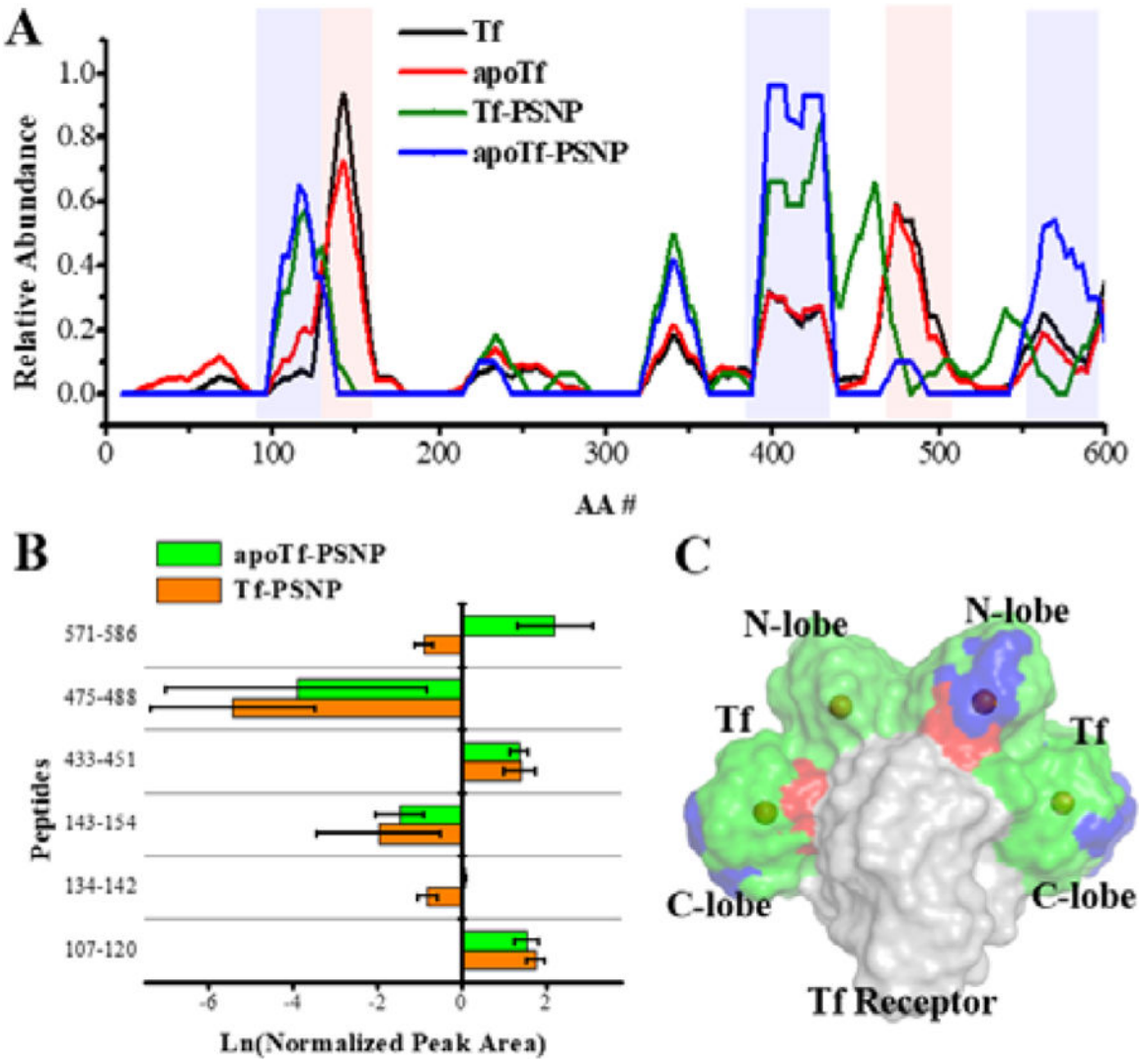

Figure 3.

(A) The RA plot for all identified cutting sites of transferrin (Tf) or apo-transferrin (apoTf) (0.2 mg/ml) with or without binding to the PSNPs (0.43 mg/ml). The RA values were averaged among three repeats. The plot was smoothed by averaging every 20 consecutive residues. (B) MS^1 peak areas of the abundant peptides found in the protein-PSNP sample normalized against that of the protein alone in natural logarithmic scale. The error bars were standard deviations calculated of 4 repeats. (C) The peptides of Tf/apoTf-PSNPs with decreased (red) or increased RA (blue) values mapped on the crystal structure (PDB: 1SUV) of Tf (green) bound with TfR (gray). Fe^{3+} ions are shown as spheres.

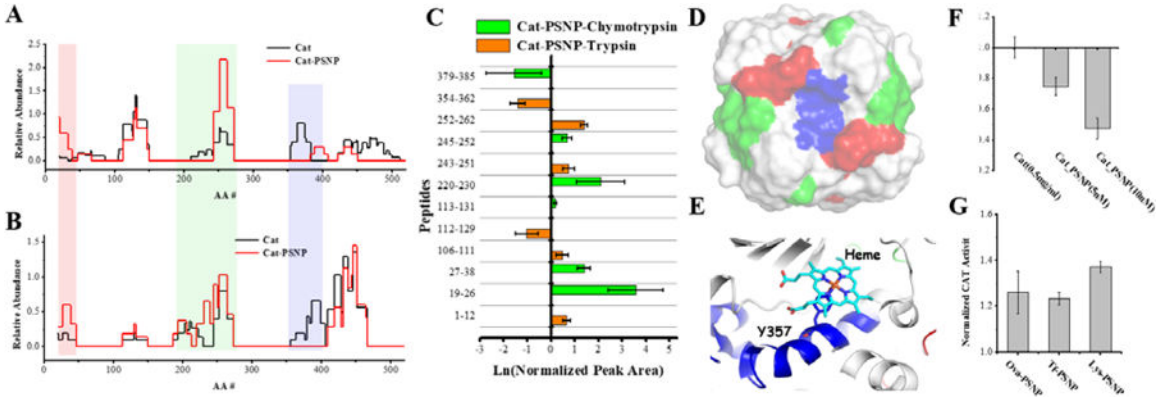

Figure 4.

The RA plot for identified (A) trypsin or (B) chymotrypsin cutting sites of catalase (Cat, 0.2 mg/ml) with or without the PSNP (0.43 mg/ml). RA values were averaged among three repeats, and the RA plots were smoothed by averaging 20 consecutive residues. (C) shows the normalized MS^1 peak area of abundant peptides in catalase with PSNPs, which were divided by the quantity of catalase without PSNPs and logarithmically scaled. (D) The peptides of Cat with PSNP showing decreased or increased RAs were mapped on the crystal structure of catalase tetramer (PDB: 1TGU). The regions highlighted in red, green, and blue, were the ones shaded by the same colored in (A) and (B). (E) The zoom-in view of the heme group of catalase. (F) The normalized activity of catalase incubated with different amounts of the PSNPS. (G) The normalized activity of catalase (0.5 mg/ml) incubated with a second protein (0.5 mg/ml) and PSNP (0.43 mg/ml) at the same time. The activity of Cat alone was normalized to 1. The error bars in (C), (F), and (G), were standard deviations of 4 repeats.

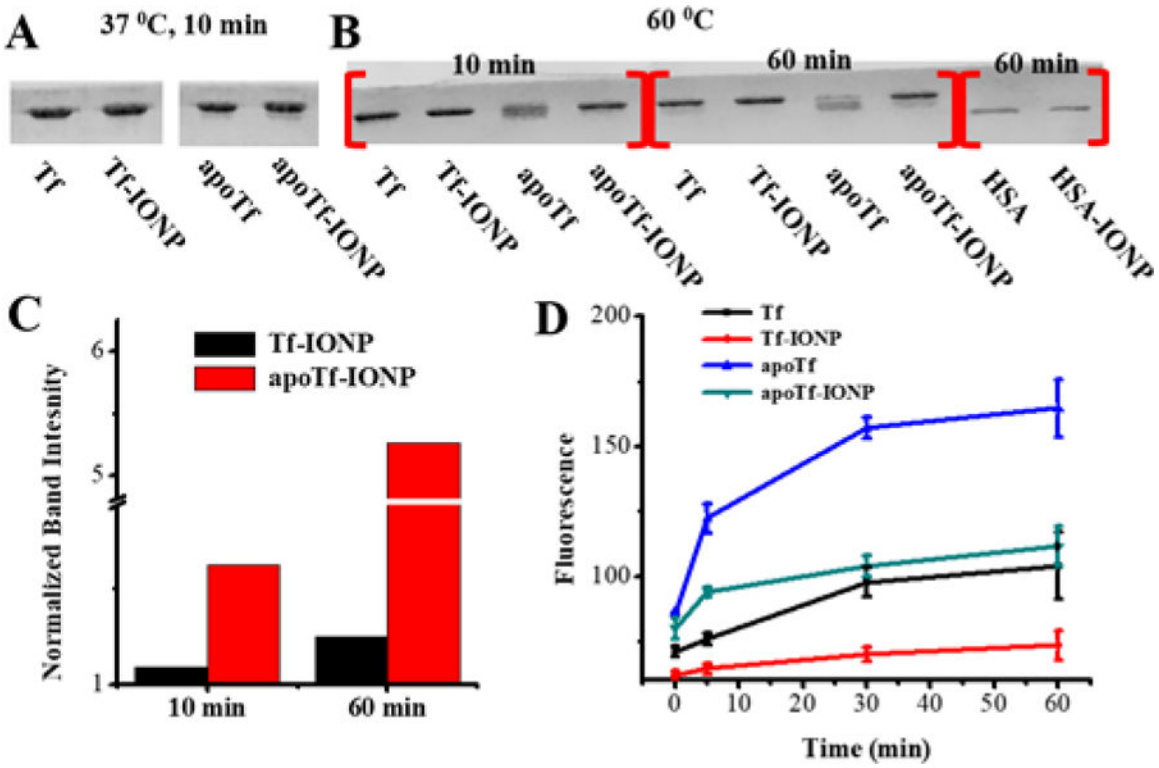

Figure 5.

(A-B) The impact on the proteolysis efficiency on transferrin Tf), apo-transferrin (apoTf), or HSA, upon adsorption onto the IONPs. The amount of the protein remaining after a 10- or 60- min trypsin digestion, was revealed by the intact protein band intensity obtained with SDS-PAGE. The protein/IONPs complex were incubated at 37 °C for 1 hr, followed by another 5 min incubation at (A) 37 °C or (B) 60 °C, before adding trypsin. Trypsin was added in 1:50 mass ratio of the protein. (C) The band intensity of impacted Tf and apoTf were quantified via ImageJ. The normalization was done by dividing the signal of protein with IONPs by that of protein alone at the corresponding time point. (D) The digestion process of protein (Tf or apoTf) with IONPs was monitored by fluorescamine labeling. Fluorescamine was added to a final concentration of 1 mM at different time points (0–60 min). The error bars were standard deviations of 3 repeats.

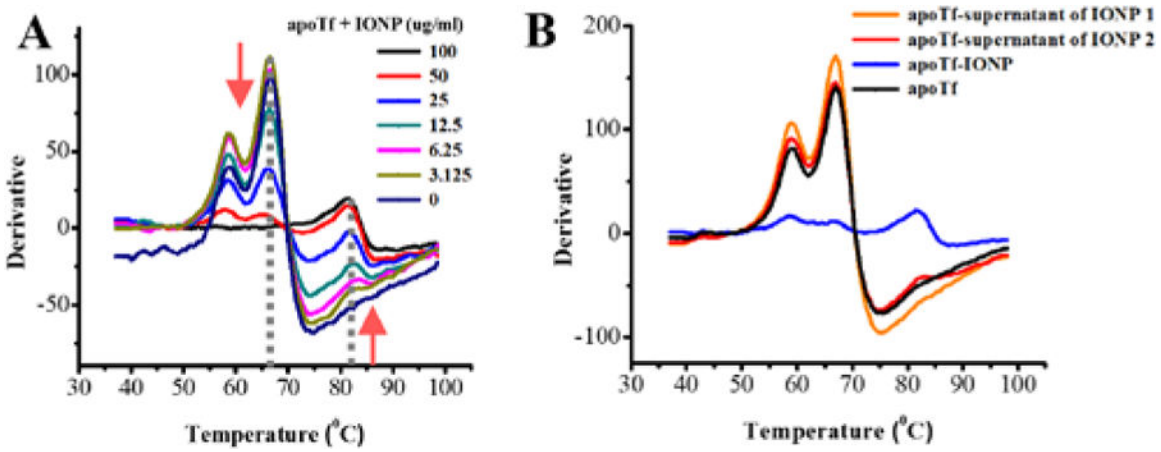

Figure 6.

The melting curves of apo-transferrin (apoTf, 0.2 mg/ml) incubated with (A) different concentration of IONPs and (B) the supernatant of IONPs (0.1 mg/ml). SYPRO Orange was added to the solution after 1 hr incubation. Excitation was at 488 nm, and the range of emission filter was 515–545 nm. The Y-axis is the first order derivative of the fluorescence intensity.

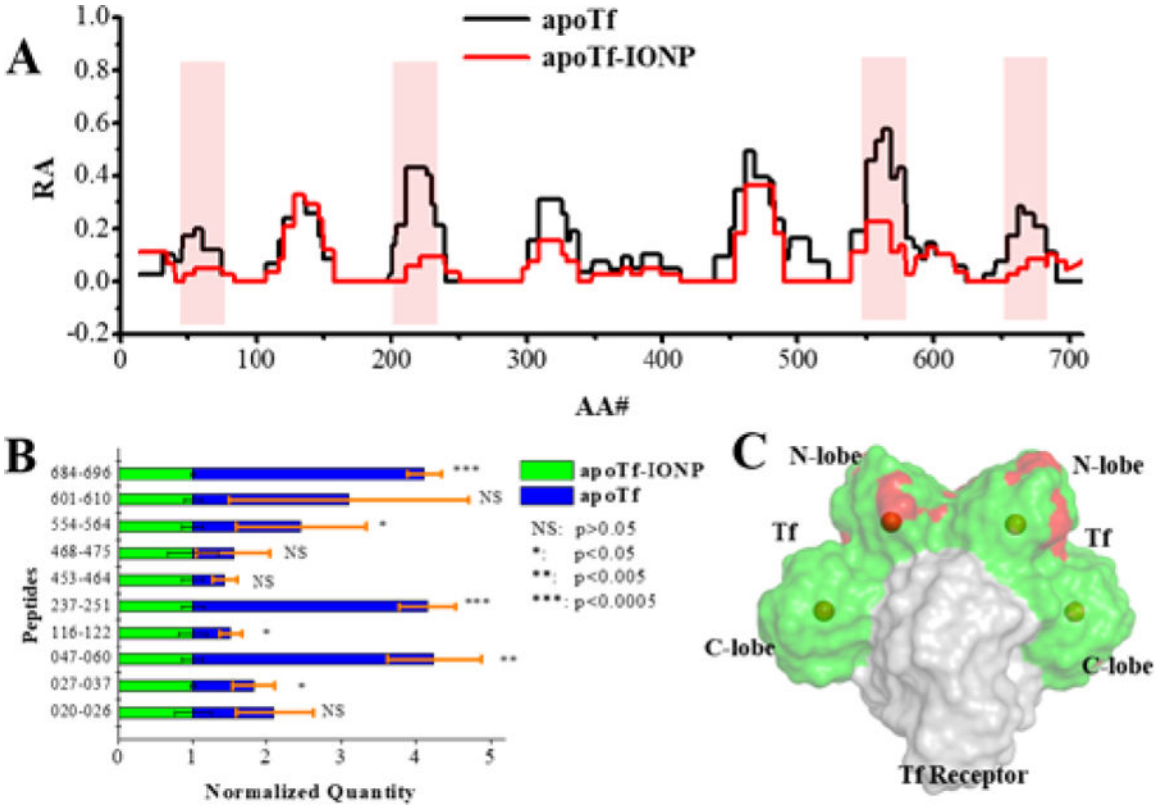

Figure 7.

(A) The RA plot for identified trypsin cutting sites of apo-transferrin (apoTf, 0.2 mg/ml) with or without the IONPs (0.1 mg/ml). RA values were averaged among three repeats, and the RA plots were smoothed by averaging 20 consecutive residues. (B) shows the normalized MS^1 peak areas of the most abundant peptides in apoTf against those of apoTf with IONPs which were scaled to 1. The error bars were standard deviations of 4 repeats. (C) The peptides of apoTf-IONPs with decreased RA (red) were located on the crystal structure (PDB: 1SUV) of Tf (green) with TfR (gray).

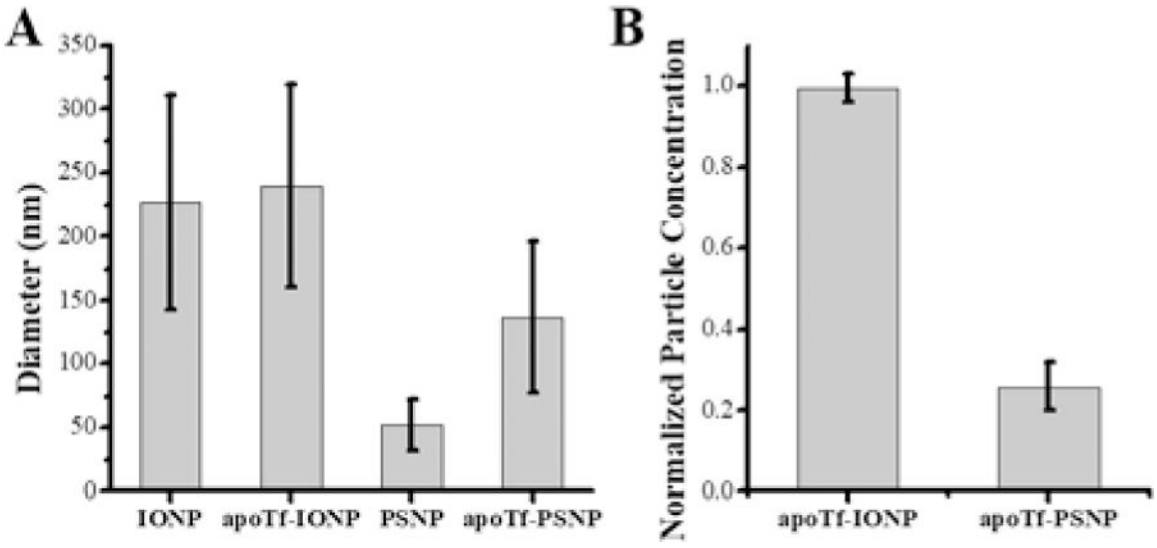

Figure 8.

(A) The hydrodynamic diameter of PSNPs or IONPs incubated with apoTf. (B) The normalized particle concentrations of PSNPs or IONPs incubated with apo-transferrin (apoTf), normalized to the concentration of the corresponding NM alone. Both (A) and (B) were measured by NTA. The error bars were standard deviations of 3 repeats.